



CERN-EP-2016-xxx  
5 December 2016

## Systematic studies of correlations between different order flow harmonics in Pb–Pb collisions at $\sqrt{s_{\text{NN}}} = 2.76$ TeV

ALICE Collaboration\*

### Abstract

The correlations between event-by-event fluctuations of anisotropic flow harmonic amplitudes have been measured in Pb–Pb collisions at  $\sqrt{s_{\text{NN}}} = 2.76$  TeV with the ALICE detector at the Large Hadron Collider. The results were obtained with the multi-particle correlation observables dubbed symmetric cumulants. These observables are robust against biases originating from non-flow effects. The centrality dependence of correlations between the higher order harmonics ( $v_3$ ,  $v_4$  and  $v_5$ ) and the lower order harmonics ( $v_2$  and  $v_3$ ), as well as the transverse momentum dependence of correlations between  $v_3$  and  $v_2$  and between  $v_4$  and  $v_2$  are presented. The results are compared to calculations from viscous hydrodynamics and A Multi-Phase Transport (AMPT) model calculations. The comparisons to viscous hydrodynamic models demonstrate that the different order harmonic correlations respond differently to the initial conditions and the temperature dependence of the ratio of shear viscosity to entropy density ( $\eta/s$ ). A small  $\eta/s$  is favored regardless of initial conditions and the AMPT initial condition yields results closest to the measurements. Correlations between the magnitudes of  $v_2$ ,  $v_3$  and  $v_4$  magnitudes show moderate  $p_T$  dependence in mid-central collisions. This might be an indication of possible viscous corrections to the equilibrium distribution at hadronic freeze-out, which might help to understand the possible contribution of bulk viscosity in the hadronic phase of the system. Together with existing measurements of individual flow harmonics, the results presented here provide further constraints on initial conditions and the transport properties of the system produced in heavy-ion collisions.

## 1 Introduction

The main emphasis of the ultra-relativistic heavy-ion collision programs at the Relativistic Heavy Ion Collider (RHIC) and the Large Hadron Collider (LHC) is to study the deconfined phase of strongly interacting nuclear matter, the Quark-Gluon Plasma (QGP). This matter exhibits strong collective and anisotropic flow in the plane transverse to the beam direction, which is driven by anisotropic pressure gradients, resulting in more particles emitted in the direction of the largest gradients. The large elliptic flow discovered at RHIC energies [1] is also observed at LHC energies [2, 3]. This has been predicted by calculations utilizing viscous hydrodynamics [4–9]. These calculations also demonstrated that the shear viscosity to the entropy density ratio ( $\eta/s$ ) of the QGP in heavy-ion collisions at RHIC and LHC energies is close to a universal lower bound  $1/4\pi$  [10].

The temperature dependence of  $\eta/s$  has some generic features that most known fluids obey. For instance, one such general behavior is that the ratio typically reaches its minimum value close to the phase transition region [11]. It was shown, using kinetic theory and quantum mechanical considerations [12], that  $\eta/s \sim 0.1$  would be the correct order of magnitude for the lowest possible shear viscosity to entropy density ratio value found in nature. Later it was demonstrated that an exact lower bound  $(\eta/s)_{\min} = 1/4\pi \approx 0.08$  can be calculated using AdS/CFT correspondence [10]. Hydrodynamical simulations also support the view that  $\eta/s$  of the QGP is close to that limit [8]. This may have important implications for other fundamental physics goals. It is argued that such a low value might imply that thermodynamic trajectories for the expanding matter would lie close to the quantum chromodynamics (QCD) critical end point, which is another subject of intensive experimental study [11, 13].

Anisotropic flow [14] is traditionally quantified with  $n^{\text{th}}$ -order flow coefficients  $v_n$  and corresponding symmetry plane angles  $\Psi_n$  in a Fourier decomposition of the particle azimuthal distribution in the plane transverse to the beam direction [15]:

$$E \frac{d^3N}{dp^3} = \frac{1}{2\pi} \frac{d^2N}{p_T dp_T d\eta} \left\{ 1 + 2 \sum_{n=1}^{\infty} v_n(p_T, \eta) \cos[n(\varphi - \Psi_n)] \right\}, \quad (1)$$

where  $E$ ,  $p$ ,  $p_T$ ,  $\varphi$  and  $\eta$  are the particle's energy, momentum, transverse momentum, azimuthal angle and pseudorapidity, respectively, and  $\Psi_n$  is the azimuthal angle of the symmetry plane of the  $n^{\text{th}}$ -order harmonic.  $v_n$  can be calculated as  $v_n = \langle \cos[n(\varphi - \Psi_n)] \rangle$ , where the brackets denote an average over all particles in all events. The anisotropic flow in heavy-ion collisions is typically understood as the hydrodynamic response of the produced matter to spatial deformations of the initial energy density profile [16]. This profile fluctuates event-by-event due to fluctuating position of the constituents inside the colliding nuclei, which implies that  $v_n$  also fluctuates [17, 18]. The recognition of the importance of flow fluctuations led to the discovery of triangular and higher flow harmonics [19, 20] as well as to the correlation between different  $v_n$  harmonics [21, 22]. The higher order harmonics are expected to be sensitive to fluctuations in the initial conditions and to the magnitude of  $\eta/s$  [23, 24], while  $v_n$  correlations have the potential to discriminate between these two respective contributions [21].

Difficulties in extracting  $\eta/s$  in heavy-ion collisions can be attributed mostly to the fact that it strongly depends on the specific choice of the initial conditions in the models used for comparison [4, 24, 25]. Viscous effects also reduce the magnitude of the elliptic flow. Furthermore, the magnitude of  $\eta/s$  used in hydrodynamic calculations should be considered as an average over the temperature evolution of the expanding fireball as it is known that  $\eta/s$  depends on temperature. In addition, part of the elliptic flow can also originate from the hadronic phase [26–28]. Therefore, both the temperature dependence of  $\eta/s$  and the relative contributions from the partonic and hadronic phases should be understood better to quantify the  $\eta/s$  of the QGP.

An important input to the hydrodynamic model simulations is the initial distribution of energy density

in the transverse plane (the initial density profile), which is usually estimated from the probability distribution of nucleons in the incoming nuclei. This initial energy density profile can be quantified by calculating the distribution of the spatial eccentricity [19],

$$\varepsilon_n e^{in\Phi_n} = -\{r^n e^{in\phi}\} / \{r^n\}, \quad (2)$$

where the curly brackets denote the average over the transverse plane, i.e.,  $\{\dots\} = \int dx dy e(x, y, \tau_0) (\dots)$ ,  $r$  is the distance to the system's center of mass,  $e(x, y, \tau_0)$  is the energy density at the initial time  $\tau_0$ , and  $\Phi_n$  is the participant plane angle (see Ref. [29, 30]). There is experimental and theoretical evidence [19, 20, 31] that the harmonic coefficients,  $v_2$  and  $v_3$ , are to a good approximation linearly proportional to the deformations in the initial energy density in the transverse plane (e.g.  $v_n \propto \varepsilon_n$  for  $n=2$  or 3).  $v_4$  and higher order flow coefficients can arise from initial anisotropies in the same harmonic [19, 29, 32, 33] (linear response) or can be induced by lower-order harmonics [34, 35] (nonlinear response). The higher harmonics ( $n > 3$ ) can be understood as superpositions of linear and nonlinear responses, through which they are correlated with lower order harmonics [32, 33, 35, 36]. When the order of the harmonic is large, the nonlinear response contribution in viscous hydrodynamics is dominant and increases in more peripheral collisions [35, 36]. The magnitude of the viscous corrections as a function of  $p_T$  for  $v_4$  and  $v_5$  is sensitive to the ansatz used for the viscous distribution function, a correction for the equilibrium distribution at hadronic freeze-out [36, 37]. Hence, studies of the higher order ( $n > 3$ ) to lower order ( $v_2$  or  $v_3$ ) harmonic correlations and their  $p_T$  dependence can help to understand the viscous correction to the momentum distribution at hadronic freeze-out which is among the least understood parts of hydrodynamic calculations [30, 36].

Recently, the ALICE Collaboration measured for the first time the Symmetric 2-harmonic 4-particle Cumulants (SC), new multiparticle observables which quantify the relationship between event-by-event fluctuations of two different flow harmonics [38]. The new observables are particularly robust against few-particle non-flow correlations and they provide independent information to recently analyzed symmetry plane correlators. It was demonstrated that they are sensitive to the temperature dependence of  $\eta/s$  of the expanding medium and therefore simultaneous descriptions of correlations between different order harmonics would constrain both the initial conditions and the medium properties [38, 39]. In this article, we have extended the analysis of SC observables to higher order Fourier harmonics (up to 5<sup>th</sup> order) as well as measured the  $p_T$  dependence of correlations for the lower order harmonics ( $v_3$ - $v_2$  and  $v_4$ - $v_2$ ). We also include extensive comparisons to hydrodynamic and AMPT model calculations. In Sec. 2 we summarize our findings from the previous work [38] and present the analysis methods. The experimental setup and measurements are described in Sec. 3 and the sources of systematic uncertainties are explained in Sec. 4. The results of the measurements are presented in Sec. 5. In Sec. 6 we present comparisons to theoretical calculations. Various theoretical models used in this article are described in Sec. 6. Sec. 7 summarizes our findings.

## 2 Experimental Observables

Existing measurements provide an estimate of the average value of  $\eta/s$  of the QGP, both at RHIC and LHC energies. What remains uncertain is how the  $\eta/s$  of the QGP depends on temperature ( $T$ ). The temperature dependence of  $\eta/s$  in the QGP was discussed in [13]. The effects on hadron spectra and elliptic flow were studied in [40] for different parametrizations of  $\eta/s(T)$ . A more systematic study with event-by-event EKRT+viscous hydrodynamic calculations has just been initiated in Ref. [30], where the first (and only rather qualitative) possibilities were investigated (see Fig. 1 therein). The emerging picture is that the study of individual flow harmonics  $v_n$  alone are unlikely to reveal the details of the temperature dependence of  $\eta/s$ . It was already demonstrated in [30] that different  $\eta/s(T)$  parameterizations can lead to the same centrality dependence of individual flow harmonics. In Ref. [21] new flow observables were introduced which quantify the degree of correlation between two different harmonics  $v_m$  and  $v_n$ .

These new observables have the potential to discriminate between the contributions to anisotropic flow development from initial conditions and from the transport properties of the QGP [21]. Therefore their measurement would provide experimental constraints on theoretical predictions for the individual stages of heavy-ion system evolution independently. In addition, it turned out that correlations of different flow harmonics are sensitive to the temperature dependence of  $\eta/s$  [38], to which individual flow harmonics are weakly sensitive [30].

For reasons discussed in [38, 41], the correlations between different flow harmonics cannot be studied experimentally with the same set of observables introduced in [21]. Based on [41], new flow observables obtained from multiparticle correlations, *Symmetric Cumulants* (SC), were introduced. SC observables are nearly insensitive to nonflow and quantify the correlation of the amplitudes of two different flow harmonics. The first measurements of SC observables were recently published by the ALICE Collaboration in [38].

The SC observables are defined as:

$$\begin{aligned} \langle \langle \cos(m\varphi_1 + n\varphi_2 - m\varphi_3 - n\varphi_4) \rangle \rangle_c &= \langle \langle \cos(m\varphi_1 + n\varphi_2 - m\varphi_3 - n\varphi_4) \rangle \rangle \\ &\quad - \langle \langle \cos[m(\varphi_1 - \varphi_2)] \rangle \rangle \langle \langle \cos[n(\varphi_1 - \varphi_2)] \rangle \rangle \\ &= \langle v_m^2 v_n^2 \rangle - \langle v_m^2 \rangle \langle v_n^2 \rangle, \end{aligned} \quad (3)$$

with the condition  $m \neq n$  for two positive integers  $m$  and  $n$  (for details see Sec. IV C in [41]). In this article  $SC(m, n)$  normalized by the product  $\langle v_m^2 \rangle \langle v_n^2 \rangle$  [38, 42] is denoted by  $NSC(m, n)$ :

$$NSC(m, n) \equiv \frac{SC(m, n)}{\langle v_m^2 \rangle \langle v_n^2 \rangle}. \quad (4)$$

Normalized symmetric cumulants reflect only the strength of the correlation which is expected to be insensitive to the magnitudes of  $v_m$  and  $v_n$ , while  $SC(m, n)$  has contributions from both the correlations between the two different flow harmonics and the individual  $v_n$  harmonics. In Eq. (4) the products in the denominator are obtained from two-particle correlations using a pseudorapidity gap of  $|\Delta\eta| > 1.0$  which suppresses biases from few-particle nonflow correlations. For the two two-particle correlations which appear in the definition of  $SC(m, n)$  in Eq. (3) the pseudorapidity gap is not needed, since nonflow is suppressed by construction in this case. This was verified by HIJING model simulations in [38].

The ALICE measurements [38] have revealed that fluctuations of  $v_2$  and  $v_3$  are anti-correlated, while fluctuations of  $v_2$  and  $v_4$  are correlated in all centralities [38]. However, the details of the centrality dependence differ in the fluctuation-dominated (most central) and the geometry-dominated (mid-central) regimes [38]. The observed centrality dependence of  $SC(4, 2)$  cannot be captured by models with constant  $\eta/s$ , indicating clearly that the temperature dependence of  $\eta/s$  plays an important role. These results were also used to discriminate between different parameterizations of initial conditions. It was demonstrated that in the fluctuation-dominated regime (central collisions), MC-Glauber initial conditions with binary collision weights are favored over wounded nucleon weights [38].

### 3 Data Analysis

Data recorded by ALICE in Pb–Pb collisions at  $\sqrt{s_{NN}} = 2.76$  TeV during the 2010 heavy-ion run at the LHC is used for this analysis. Detailed descriptions of the ALICE detector can be found in [43–45]. The Time Projection Chamber (TPC) was used to reconstruct charged particle tracks and measure their momenta with full azimuthal coverage in the pseudorapidity range  $|\eta| < 0.8$ . Two scintillator arrays (V0) which cover the pseudo-rapidity ranges  $-3.7 < \eta < -1.7$  and  $2.8 < \eta < 5.1$  were used for triggering and the determination of centrality [46]. The trigger conditions and the event selection criteria are identical to those described in [2, 46]. Approximately  $10^7$  minimum-bias Pb–Pb events with a reconstructed primary

vertex within  $\pm 10$  cm from the nominal interaction point along the beam direction are selected. Charged particles reconstructed in the TPC in  $|\eta| < 0.8$  and  $0.2 < p_T < 5$  GeV/c were selected. The charged track quality cuts described in [2] were applied to minimize contamination from secondary charged particles and fake tracks. The track reconstruction efficiency and contamination were estimated from HIJING Monte Carlo simulations [47] combined with a GEANT3 [48] detector model and were found to be independent of the collision centrality. The reconstruction efficiency increases from 70% to 80% for particles with  $0.2 < p_T < 1$  GeV/c and remains constant at  $(80 \pm 5)\%$  for  $p_T > 1$  GeV/c. The estimated contamination by secondary charged particles from weak decays and photon conversions is less than 6% at  $p_T = 0.2$  GeV/c and falls below 1% for  $p_T > 1$  GeV/c. The  $p_T$  cut-off of 0.2 GeV/c reduces event-by-event biases due to small reconstruction efficiency at lower  $p_T$ , while the high  $p_T$  cut-off of 5 GeV/c reduces the effect of jets on the measured correlations. Reconstructed TPC tracks were required to have at least 70 space points (out of a maximum of 159). Only tracks with a transverse distance of closest approach (DCA) to the primary vertex less than 3 mm, both in the longitudinal and transverse directions, are accepted. This reduces the contamination from secondary tracks produced in the detector material, particles from weak decays, etc. Tracks with kinks (i.e, tracks that appear to change direction due to multiple scattering or  $K^\pm$  decays) were rejected.

#### 4 Systematic Uncertainties

The systematic uncertainties are estimated by varying the event and track selection criteria. All systematic checks described here are performed independently. The  $SC(m,n)$  values resulting from each variation are compared to ones from the default event and track selection described in the previous section, and differences are taken as the systematic uncertainty due to each individual source. The contributions from different sources were added in quadrature to obtain the total systematic uncertainty.

The event centrality was determined by the V0 detectors [49] with better than 2% resolution. The systematic uncertainty from the centrality determination was evaluated by using the TPC and Silicon Pixel Detector (SPD) [50] detectors instead of the V0 detectors. The systematic uncertainty from the centrality determination is about 3% both for  $SC(5,2)$  and  $SC(4,3)$ , and 8% for  $SC(5,3)$ .

As described in Sec. 3, the reconstructed vertex position along the beam axis ( $z$ -vertex) is required to be located within 10 cm of the interaction point (IP) to ensure uniform detector acceptance for tracks within  $|\eta| < 0.8$ . The systematic uncertainty from the  $z$ -vertex cut was estimated by reducing the  $z$ -vertex range to 8 cm and was found to be less than 3%.

The analyzed events were recorded with two settings of the magnet polarity and the resulting data sets have almost equal numbers of events. Events with both magnet polarities were used in the default analysis, and the systematic uncertainties were evaluated from the variation between each of the two magnetic field settings. The uncertainty on the  $p_T$  dependent track reconstruction efficiency was also taken into account. Magnetic polarity variation and reconstruction efficiency effects contribute less than 2% to the systematic uncertainty.

The systematic uncertainty due to the track reconstruction was estimated from comparisons between results for the so-called standalone TPC tracks with the same parameters as described in Sec. 3, and tracks from a combination of the TPC and the Inner Tracking System (ITS) detectors with tighter selection criteria. To correct for non-uniform azimuthal acceptance due to dead zones in the SPD, and to get the best transverse momentum resolution, approach of hybrid selection with SPD hit and/or ITS refit tracks combined with TPC were used. Then each track reconstruction strategy was evaluated by varying the threshold on parameters used to select the tracks at the reconstruction level. The systematic difference of up to 12% was observed in  $SC(m,n)$  from the different track selections. In addition, we applied the like-sign technique to estimate non-flow contributions to  $SC(m,n)$ . The difference between results obtained by selecting all charged particles and results obtained after either selecting only positively or

only negatively charged particles was the largest contribution to the systematic uncertainty and it is about 7% for SC(4,3) and 20% for SC(5,3).

Another large contribution to the systematic uncertainty originates from azimuthal non-uniformities in the efficiency. In order to estimate its effects, we use the AMPT model (see Sec. 6) which has a uniform distribution in azimuthal angle. Detector inefficiencies were introduced to mimic the non-uniform azimuthal distribution in the data. For the observables SC(5,2), SC(5,3) and SC(4,3) the variation due to non-uniform acceptance is about 9%, 17% and 11%, respectively. Overall, the systematic uncertainties are larger for SC(5,3) and SC(5,2) than for the lower harmonics of SC( $m,n$ ). This is because  $v_n$  decreases with increasing  $n$  and becomes more sensitive to azimuthal modulation due to detector imperfections.

## 5 Results

The centrality dependence of the higher order harmonic correlations (SC(4,3), SC(5,2) and SC(5,3)) are presented in Fig. 1 and compared to the lower order harmonic correlations (SC(4,2) and SC(3,2)) which were measured in [38]. The correlation between  $v_3$  and  $v_4$  is negative, and similarly for  $v_3$  and  $v_2$ , while the other correlations are all positive, which reveals that  $v_2$  and  $v_5$  as well as  $v_3$  and  $v_5$  are correlated like  $v_2$  and  $v_4$ , while  $v_3$  and  $v_4$  are anti-correlated like  $v_3$  and  $v_2$ .

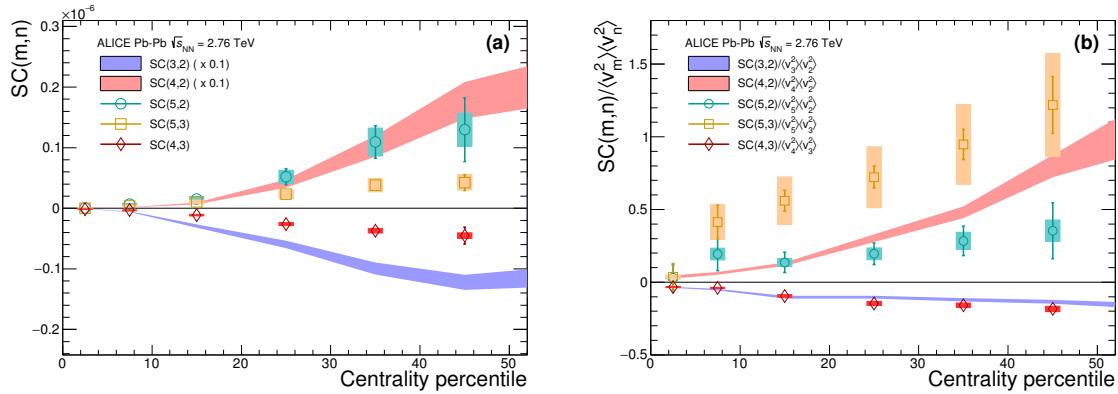


**Fig. 1:** SC( $m,n$ ) (a) and NSC( $m,n$ ) (b) with flow harmonic up to 5<sup>th</sup> order in Pb–Pb collisions at  $\sqrt{s_{NN}} = 2.76$  TeV. The lower order harmonic correlations (SC(3,2), SC(4,2), NSC(3,2) and NSC(4,2)) are taken from [38] and shown as bands. Note that the systematic and statistical errors are combined in quadrature for these lower order harmonic correlations and SC(4,2) and SC(3,2) are scaled by a factor of 0.1.

The higher order flow harmonic correlations (SC(4,3), SC(5,2) and SC(5,3)) are much smaller compared to the lower order harmonic correlations. In particular SC(5,2) is 10 times smaller than SC(4,2) and SC(4,3) is about 20 times smaller than SC(3,2).

However, unlike SC( $m,n$ ), the NSC( $m,n$ ) results with the higher order flow harmonics show almost the same order of the correlation strength as the lower order flow harmonic correlations (NSC(3,2) or NSC(4,2)). The NSC(4,3) magnitude is comparable to NSC(3,2) and one finds that a hierarchy, NSC(5,3) > NSC(4,2) > NSC(5,2), holds for centrality ranges > 20% within the errors as shown in Fig. 1b. These results indicate that the lower order harmonic correlations are larger than higher order harmonic correlations, not only because of the correlation strength itself but also because of the strength of the individual flow harmonics. SC(5,2) is stronger than SC(5,3), but the normalized correlation between  $v_5$  and  $v_3$  is stronger than the normalized correlation between  $v_5$  and  $v_2$ .

It can be seen in Fig. 1a that the lower order harmonic correlations (SC(3,2) and SC(4,2)) and SC(5,2) increase non-linearly toward peripheral collisions. In case of SC(5,3) and SC(4,3), the centrality depen-

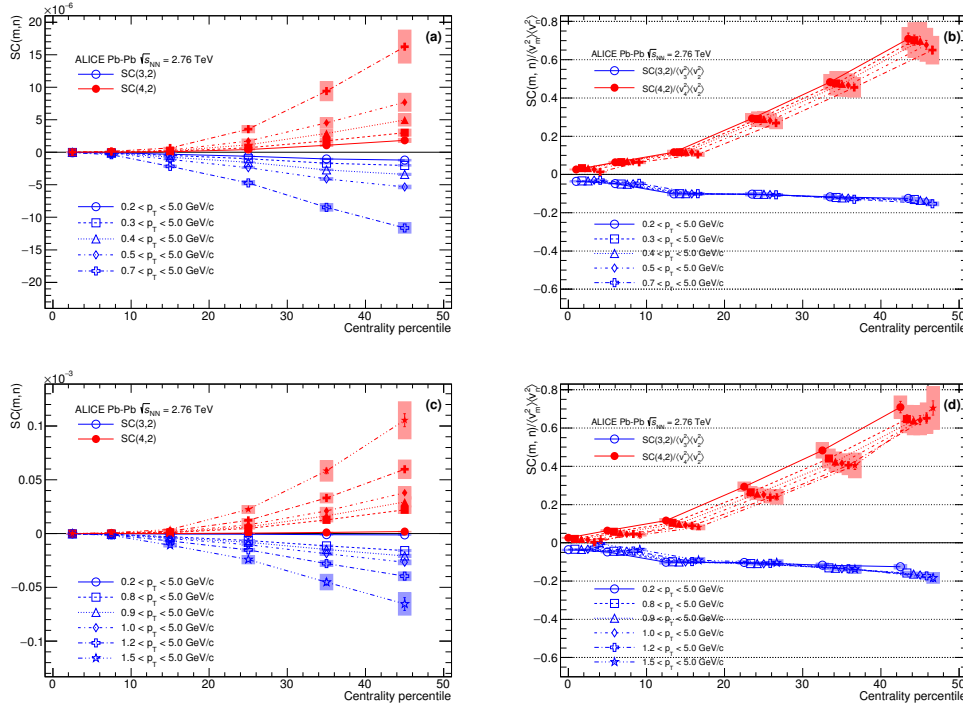


**Fig. 2:** SC(3,2) and SC(4,2) with various minimum  $p_T$  cuts ((a) and (c)) and results of normalized SC(3,2) and SC(4,2) ((b) and (d)) in Pb–Pb collisions at  $\sqrt{s_{NN}} = 2.76$  TeV. The panel (a) and (b) show the results for minimum  $p_T$  range,  $0.2 < p_T < 0.7$  GeV/c and the panel (c) and (d) are for minimum  $p_T$  range,  $0.8 < p_T < 1.5$  GeV/c. Note that NSC data points from each minimum  $p_T$  in a centrality percentile bin are shifted for visibility.

dence is weaker than the other harmonic correlations and a monotonic increase is observed for these harmonic correlations. NSC(5,3) shows the strongest correlation among all harmonics and NSC(4,2), NSC(5,2) shows a weak centrality dependence. Both NSC(3,2) and NSC(4,3) show a monotonic increase toward peripheral collisions with the similar magnitude.

To study the  $p_T$  dependence of  $SC(m,n)$ , we change the low  $p_T$  cut-off, instead of using independent  $p_T$  interval, in order to avoid large statistical fluctuations in the results. Various minimum  $p_T$  cuts from 0.2 to 1.5 GeV/c are applied. The results of  $p_T$  dependence of SC(3,2) and SC(4,2) with minimum  $p_T$  cuts,  $0.2 < p_T < 0.7$  GeV/c, are shown on the panel (a) in Fig. 2. The strength of  $SC(m,n)$  becomes larger as the minimum  $p_T$  increases. This  $p_T$  dependent correlations have much stronger centrality dependence, where  $SC(m,n)$  gets much larger as the centrality or the minimum  $p_T$  cut increase. NSC(3,2) and NSC(4,2) with different minimum cuts are shown on the panel (b) and (d) in Fig. 2. The strong  $p_T$  dependence observed in  $SC(m,n)$  is not seen in  $NSC(m,n)$ . The  $NSC(m,n)$  results are aligned all together and consistent in errors for all minimum  $p_T$  cuts. This indicates that the  $p_T$  dependence of  $SC(m,n)$  is dominated by the  $p_T$  dependence of  $\langle v_n \rangle$  values. The minimum  $p_T$  cuts are extended from 0.8 to 1.5 GeV/c and the results are shown on the panel (c) and (d) in Fig. 2. While  $SC(m,n)$  show the similar trends as for  $p_T < 0.8$  GeV/c,  $NSC(m,n)$  tends to decrease with increasing  $p_T$  or the centrality. The  $p_T$  dependence for NSC(3,2) is not clearly seen and it is consistent with no  $p_T$  dependence within the current statistical and systematic errors for the centrality range  $< 30\%$  and shows moderate decreasing trend for increasing  $p_T$  for  $> 30\%$  centrality range. NSC(4,2) shows a moderate decreasing trend as  $p_T$  or the centrality increase. These observations are strikingly different from  $p_T$  dependence of individual flow harmonics, where the relative flow fluctuations  $\sigma_{v_2}/\langle v_2 \rangle$  [51] are independent of momentum up to  $p_T \sim 8$  GeV/c (see Fig. 3 in Ref. [52]).

## 6 Model Comparisons

We have compared the centrality dependence of our observables with the event-by-event EKRT+viscous hydrodynamic calculations [30], where the initial energy density profiles are calculated using a next-to-leading order perturbative-QCD+saturation model [53, 54]. The subsequent spacetime evolution is described by relativistic dissipative fluid dynamics with different parameterizations for the temperature dependence of the shear viscosity to entropy density ratio  $\eta/s(T)$ . This model gives a good description of the charged hadron multiplicity and the low  $p_T$  region of the charged hadron spectra at RHIC and the LHC (see Fig. 11-13 in [30]). Each of the  $\eta/s(T)$  parameterizations is adjusted to reproduce the measured  $v_n$  from central to mid-peripheral collisions (see Fig. 14 in [30]).

The VISH2+1 [55, 56] event-by-event calculations for relativistic heavy-ion collisions are based on (2+1)-dimensional viscous hydrodynamics which describes both the QGP phase and the highly dissipative and even off-equilibrium late hadronic stage with fluid dynamics. With well tuned transport coefficients, decoupling temperature and given initial condition discussed later, it could describe the  $p_T$  spectra and different flow harmonics at RHIC and the LHC [5, 55, 57, 58]. Three different initial conditions (MC-Glauber, MC-KLN and AMPT) along with different constant  $\eta/s$  values are used in the model [39]. Traditionally, the Glauber model constructs the initial entropy density from contributions of the wounded nucleon and binary collision density profiles [59], and the KLN model assumes that the initial entropy density is proportional to the initial gluon density calculated from the corresponding  $k_T$  factorization formula [60]. In the Monte Carlo versions (MC-Glauber and MC-KLN) [61–63], additional initial state fluctuations are introduced through the position fluctuation of individual nucleons inside the colliding nuclei. For the AMPT initial conditions [58, 64, 65], the fluctuating energy density profiles are constructed from the energy decompositions of individual partons, which fluctuate in both momentum and position coordinate. Compared with the MC-Glauber and MC-KLN initial conditions, the additional Gaussian smearing in the AMPT initial conditions gives rise to non-vanishing initial local flow velocities [64].

The centrality dependence of SC observables is compared to that in the AMPT model [66–68]. Even though thermalization could be achieved in collisions of very large nuclei and/or at extremely high energy [69], the dense matter created in heavy-ion collisions may not reach full thermal or chemical equilibrium as a result of its finite volume and short time scale. To address such non-equilibrium many-body dynamics, AMPT has been developed, which includes both initial partonic and final hadronic interactions and the transition between these two phases of matter. For the initial conditions, the AMPT model uses the spatial and momentum distributions of hard minijet partons and soft strings from the HIJING model [47, 70]. The AMPT model can be run in two main configurations, the default and the string melting model<sup>1</sup>. In the default version, partons are recombined with their parent strings when they stop interacting. The resulting strings are later converted into hadrons using the Lund string fragmentation model [71, 72]. In the string melting version, the initial strings are melted into partons whose interactions are described by the ZPC parton cascade model [73]. These partons are then combined into the final state hadrons via a quark coalescence model. In both configurations, the dynamics of the subsequent hadronic matter is described by a hadronic cascade based on A Relativistic Transport (ART) model [74] which also includes resonance decays. The third version used in this article is based on the string melting configuration, in which the hadronic rescattering phase is switched off to study its influence to the development of anisotropic flow. Even though the string melting version of AMPT [68, 75] reasonably reproduces particle yields,  $p_T$  spectra, and  $v_2$  of low- $p_T$  pions and kaons in central and mid-central Au–Au collisions at  $\sqrt{s_{NN}} = 200$  GeV and Pb–Pb collisions at  $\sqrt{s_{NN}} = 2.76$  TeV [76], it was seen clearly in the recent study [77] that it fails to quantitatively reproduce the harmonic flow coefficients of identified hadrons ( $v_2$ ,  $v_3$ ,  $v_4$  and  $v_5$ ) at  $\sqrt{s_{NN}} = 2.76$  TeV. It turns out that the radial flow in AMPT is 25% lower than the

<sup>1</sup>The input parameters used in both configurations are:  $\alpha_s = 0.33$ , a partonic cross-section of 1.5 mb, while the Lund string fragmentation parameters were set to  $\alpha = 0.5$  and  $b = 0.9 \text{ GeV}^{-2}$ .



measured value at the LHC, which indicates that the unrealistically low radial flow in AMPT is responsible for the quantitative disagreement [77]. The details of configurations of AMPT settings used for this article and the comparisons of  $p_T$  differential  $v_n$  for pions, kaons and protons to the data can be found in [77].

## 6.1 Low Order Harmonic Correlations

SC(3,2) and SC(4,2) are compared to several theoretical calculations. The event-by-event EKRT+viscous hydrodynamic predictions with the different parameterizations for the temperature dependence of the shear viscosity to entropy density ratio  $\eta/s(T)$  are shown in Fig. 2 of Ref. [38]. It has been demonstrated that NSC(3,2) observable is sensitive mainly to the initial conditions, while NSC(4,2) observable is sensitive to both the initial conditions and the system properties, which is consistent with the predictions from [21]. However, the sign of NSC(3,2) is positive in the models in 0-10% central collisions while it is negative in data. In the most central collisions the anisotropies originate mainly from fluctuations, i.e. the initial ellipsoidal geometry characteristic for mid-central collisions plays little role in this regime. This observation helps to understand better the fluctuations in initial energy density. NSC(4,2) observable shows better sensitivity for different  $\eta/s(T)$  parameterizations but the model cannot describe neither the centrality dependence nor the absolute values. This observed distinct discrepancy between data and theoretical predictions indicates that the current understanding of initial conditions used to model the initial stages of heavy-ion collision need to be revisited to further constrain the  $\eta/s(T)$ , considering the difficulties in separating the role of the  $\eta/s$  from the initial conditions to the final state particle anisotropies [4, 25]. The use of SC( $m,n$ ) and NSC( $m,n$ ) can provide new constraints on the detailed modeling of fluctuating initial conditions. The better constraints on the initial state conditions will certainly reduce the uncertainties of determining  $\eta/s(T)$ .

The results with the comparison to VISH2+1 calculation [39] are shown in Fig. 3. All calculations with large  $\eta/s$  regardless of the initial conditions ( $\eta/s = 0.2$  for MC-KLN and MC-Glauber initial conditions and  $\eta/s = 0.16$  for AMPT initial condition) fail to capture the centrality dependence of SC(3,2) and SC(4,2). Among the calculations with small  $\eta/s$  ( $\eta/s = 0.08$ ), the one with the AMPT initial condition describes the data better both for SC(3,2) and SC(4,2) in general but it cannot describe the data quantitatively for most of the centrality ranges. Similarly to the event-by-event EKRT+viscous hydrodynamic calculations [30], the sign of the normalized NSC(3,2) in the model calculations in Fig 3 is opposite to that in data in 0-10% central collisions. NSC(3,2) does not show sensitivity to the initial conditions nor to the different  $\eta/s$  parameterizations used in the models and cannot be described by these models quantitatively. However NSC(4,2) is sensitive both to the initial conditions and the  $\eta/s$  parameterizations used in the models. Even though NSC(4,2) favors both AMPT initial condition with  $\eta/s = 0.08$  and MC-Glauber initial condition with  $\eta/s = 0.20$ , SC(4,2) can be only described by smaller  $\eta/s$  from AMPT and MC-Glauber initial conditions. Hence these calculations with large  $\eta/s = 0.20$  are ruled out. We conclude that  $\eta/s$  should be small and AMPT initial condition is favored by the data.

The SC( $m,n$ ) calculated from AMPT simulations are compared to data in Fig. 4. As for SC(3,2), none of the calculations can describe the data and the calculation with the default AMPT setting follows the trend of the data closest. The same default calculation can describe the sign and magnitude of NSC(3,2) while the hydrodynamic calculations failed to describe either of them in the most central collisions. Interestingly the string melting AMPT model cannot reproduce the data and the strength of the correlation is weaker than in data. The third version based on the string melting configuration without the hadronic rescattering phase is also shown. The hadronic rescattering stage makes both SC(3,2) and NSC(3,2) stronger in the string melting AMPT model but not enough to describe the data. Further we investigated why the default AMPT model can describe NSC(3,2) fairly well but underestimates SC(3,2). By taking the differences in the individual flow harmonics ( $v_2$  and  $v_3$ ) between the model and data into account, we were able to recover the difference in SC(3,2) between the data and the model. The discrepancy in SC(3,2) can be explained by the overestimated individual  $v_n$  values reported in [77] in all the centrality

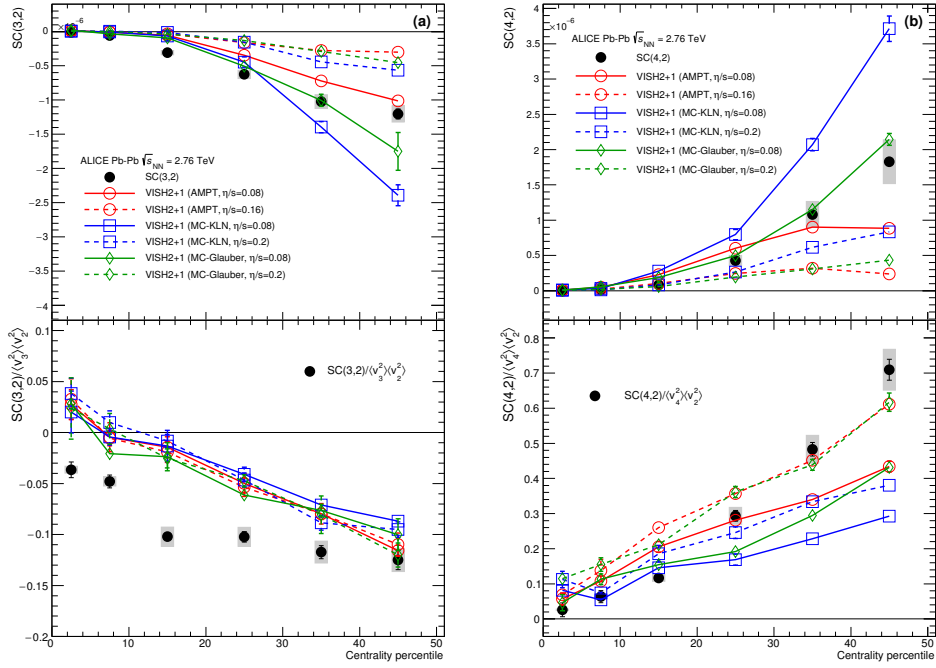


**Fig. 3:**  $SC(3,2)$  (a) and  $SC(4,2)$  (b) in Pb–Pb collisions at  $\sqrt{s_{NN}} = 2.76$  TeV are compared to various VISH2+1 calculations [39] with different settings. Upper (lower) panels show  $SC(m,n)$  ( $NSC(m,n)$ ). Calculations with three initial conditions from AMPT, MC-KLN, and MC-Glauber are drawn as different colors and markers. The  $\eta/s$  parameters are shown in line styles, the small  $\eta/s = 0.08$  are shown as solid lines, and large  $\eta/s = 0.2$  for MC-KLN and MC-Glauber, 0.16 for AMPT are drawn as dashed lines.

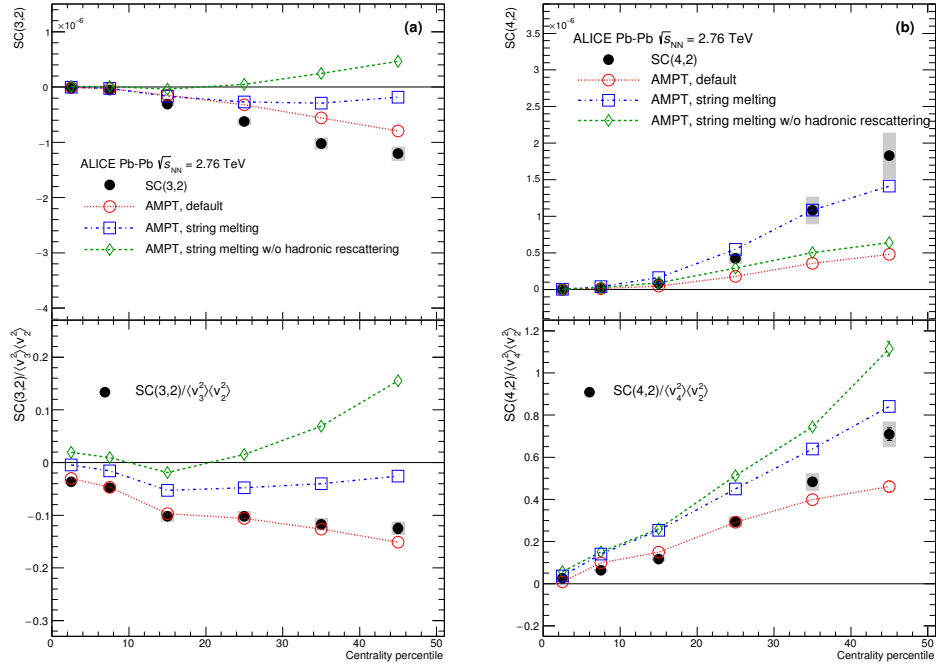


**Fig. 4:**  $SC(3,2)$  (a) and  $SC(4,2)$  (b) in Pb–Pb collisions at  $\sqrt{s_{NN}} = 2.76$  TeV are compared to various AMPT models. Upper panels (lower) are the results of  $SC(m,n)$  ( $NSC(m,n)$ ).

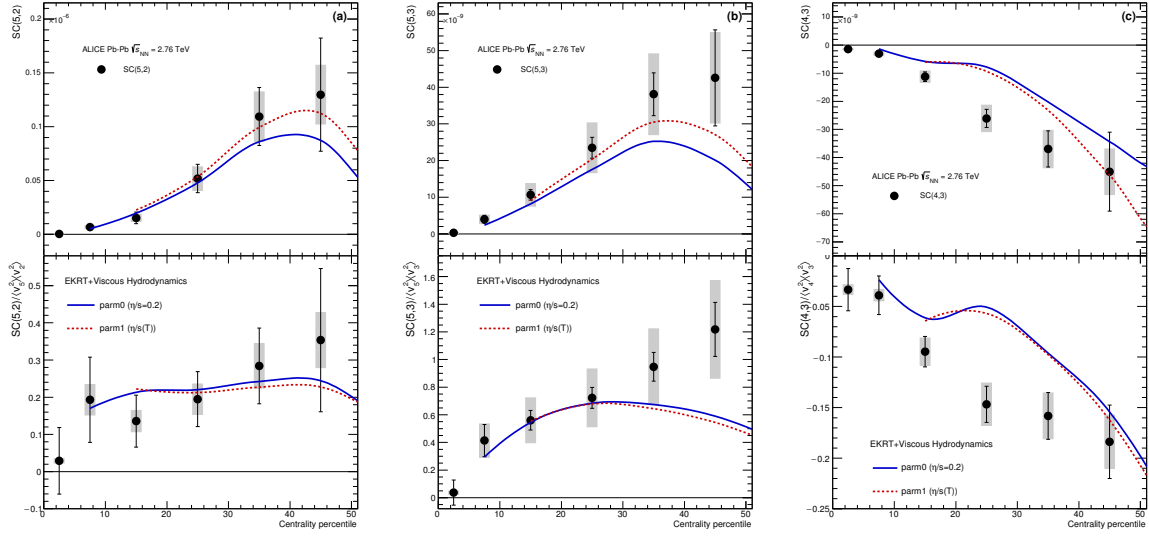


**Fig. 5:** Results of SC(5,2), SC(5,3) and SC(4,3) in Pb–Pb collisions at  $\sqrt{s_{\text{NN}}} = 2.76$  TeV are compared to the event-by-event EKRT+viscous hydrodynamic calculations [30]. The dashed lines are hydrodynamic predictions with various  $\eta/s(T)$  parameterizations [30]. These SC(3,2) and SC(4,2) will be replaced with new figures for higher order correlations once we have the calculations from Harri Niemi et. al [30].

ranges.

In the case of SC(4,2), the string melting AMPT model can fairly well describe the data while the default model underestimates it. NSC(4,2) is slightly overestimated by the same setting which can describe SC(4,2) but the default AMPT model can describe the data better. The influence of the hadronic rescattering phase for NSC(4,2) is opposite to other observables (SC(3,2), NSC(3,2) and SC(4,2)). The hadronic rescattering makes NSC(4,2) slightly smaller. It should be noted that the better agreement for SC( $m,n$ ) should not be overemphasized since there are discrepancies in the individual  $v_n$  between the AMPT models and the data as it was demonstrated for SC(3,2). Hence the simultaneous description of SC( $m,n$ ) and NSC( $m,n$ ) should give better constraints to the parameters in AMPT models.

## 6.2 Higher Order Harmonic Correlations

The higher order harmonic correlations (SC(4,3), SC(5,2) and SC(5,3)) are compared to several theoretical calculations. The event-by-event EKRT+viscous hydrodynamic predictions with the different parameterizations for the temperature dependence of the shear viscosity to entropy density ratio  $\eta/s(T)$  are shown in Fig. 5. While we discussed the comparison to these hydrodynamic model calculations with various temperature dependent  $\eta/s$ , only two calculations with the parameters which describe the lower order harmonic correlations better are compared to the higher order harmonic correlations. The other calculations show a quite clear deviation from the data. As it is seen in Fig. 1 from Ref. [30] that the temperature at the minimum of  $\eta/s$  for “parm1” is smaller than the other parameters used. The model calculations with the parameters whose temperature at the minimum of  $\eta/s$  is larger than “parm1” can be ruled out. The correlations between  $v_5$  and  $v_2$  and between  $v_5$  and  $v_3$  are described better than the lower order harmonic correlations by these calculations. In the case of the correlation between  $v_4$  and  $v_3$ , the same models underestimate the data significantly like the correlation between  $v_3$  and  $v_2$ .

The higher order harmonic correlations (SC(4,3), SC(5,2) and SC(5,3)) are compared to VISH2+1 calculations [39], shown in Fig. 6. All the models with large  $\eta/s$  regardless of the initial conditions ( $\eta/s = 0.2$  for MC-KLN and MC-Glauber, and  $\eta/s = 0.16$  for AMPT initial conditions) failed to capture the centrality dependence of SC(5,2), SC(5,2) and SC(5,3), more clearly than for the lower order harmonic

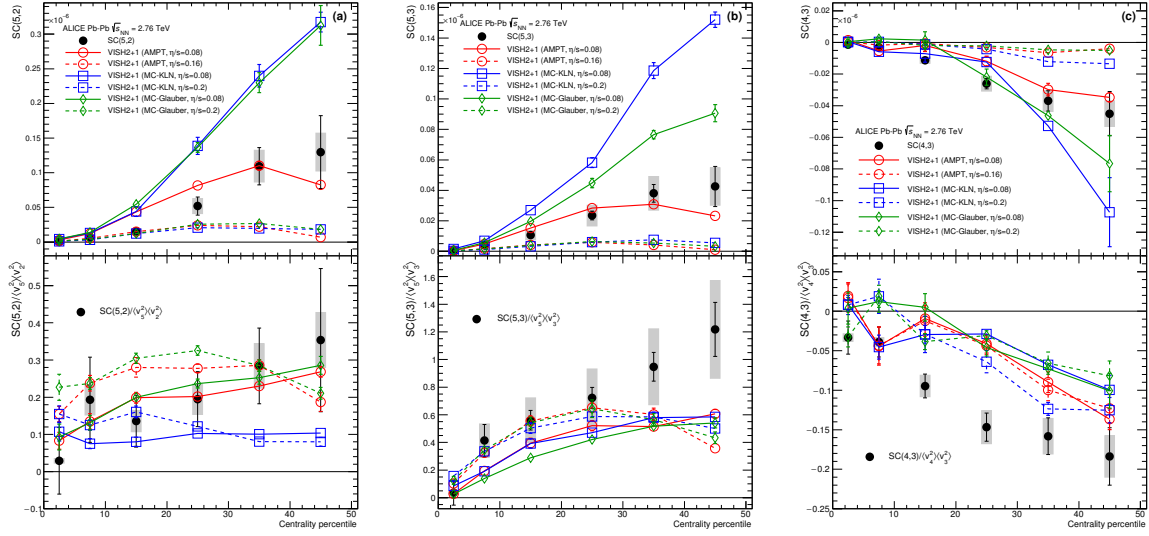


**Fig. 6:** Results of  $SC(5,2)$ ,  $SC(5,3)$  and  $SC(4,3)$  in Pb–Pb collisions at  $\sqrt{s_{NN}} = 2.76$  TeV are compared to various VISH2+1 calculations [39]. Three initial conditions from AMPT, MC-KLN and MC-Glauber are drawn as different colors and markers. The  $\eta/s$  parameters are shown as different line styles, the small shear viscosity ( $\eta/s = 0.08$ ) are shown as solid lines, and large shear viscosities ( $\eta/s = 0.2$  for MC-KLN and MC-Glauber, 0.16 for AMPT) are drawn as dashed lines. Upper panels are the results of  $SC(m,n)$  and lower panels are the results of  $NSC(m,n)$ .

correlations ( $SC(3,2)$  and  $SC(4,2)$ ). Among the models with small  $\eta/s$  ( $\eta/s = 0.08$ ), the one from the AMPT initial condition describes the data much better than the ones with other initial conditions. A quite clear separation between different initial conditions is observed for these higher order harmonic correlations compared to the lower order harmonic correlations.  $NSC(5,2)$  and  $SC(5,3)$  are quite sensitive to both the initial conditions and the  $\eta/s$  parameterizations. Similarly as the above mentioned hydrodynamic calculations [30], the sign of the  $NSC(4,3)$  in these models is opposite to its signature in the data in 0-10% central collisions.  $NSC(4,3)$  shows sensitivity to both initial conditions and  $\eta/s$  parameterizations.  $SC(4,3)$  data is clearly favored by smaller  $\eta/s$  but  $NSC(4,3)$  cannot be described by these models quantitatively.

The extracted results for final state particles from AMPT simulations in the same way as for the data are compared in Fig. 7. The string melting AMPT model describes  $SC(5,3)$  and  $NSC(5,3)$  well. The same setting overestimates  $SC(5,2)$  and  $NSC(5,2)$ . However the default AMPT model can describe  $NSC(5,3)$  and  $NSC(5,2)$  fairly well as it is the case for  $NSC(3,2)$  and  $NSC(4,2)$  seen in Fig. 4. In the case of  $SC(4,3)$ , neither of the settings can describe the data but the default AMPT model follows the data closest. The string melting AMPT model fails to describe  $SC(4,3)$  and  $NSC(4,3)$ . In summary, the default AMPT model describes well the normalized symmetric cumulants ( $NSC(m,n)$ ) from lower to higher order harmonic correlations while the string melting AMPT model overestimates  $NSC(5,2)$  and underestimates (or predicts very weak correlation)  $NSC(4,3)$ .

As discussed in Sec. 5, a hierarchy  $NSC(5,3) > NSC(4,2) > NSC(5,2)$  holds for centrality ranges  $> 20\%$  within the errors and  $NSC(5,2)$  is smaller than  $NSC(5,3)$  while  $SC(5,2)$  is larger than  $SC(5,3)$ . Except for 0-10% centrality range, we found that the same hierarchy also holds for the hydrodynamic calculations and the AMPT models in this article. The observed difference between  $SC(5,2)$  and  $SC(5,3)$  ( $SC(5,2) > SC(5,3)$ ) can be explained by the difference of the individual flow harmonics ( $v_2 > v_3$ ). The opposite trend are observed for the normalized SC ( $NSC(5,3) > NSC(5,2)$ ). This can be attributed to the fact that the flow fluctuation is stronger for  $v_3$  than  $v_2$  [78]. It was claimed in Ref. [39] and seen also in

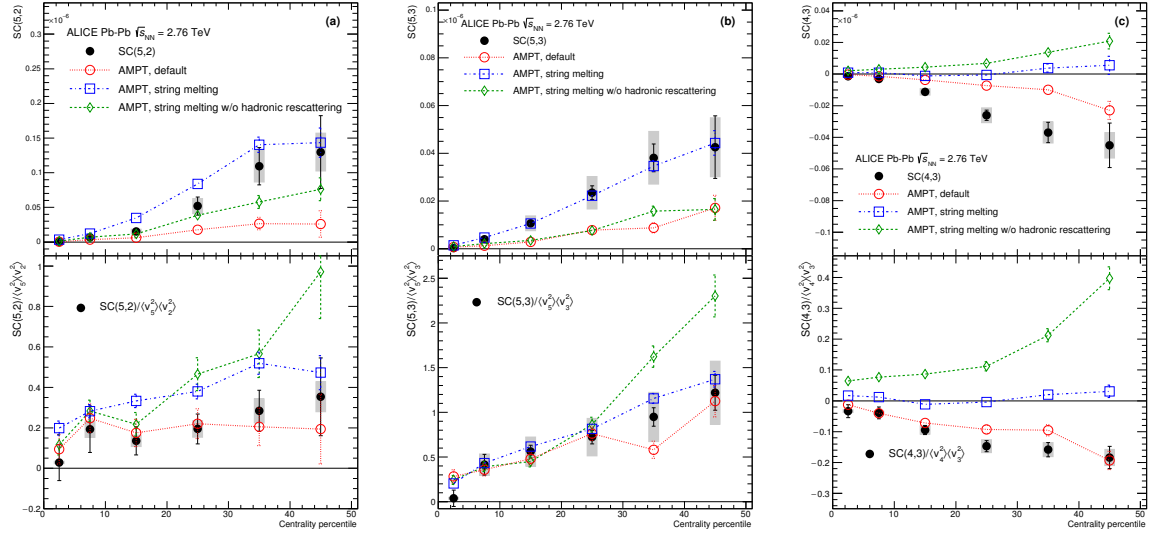


**Fig. 7:** Results of SC(5,2), SC(5,3) and SC(4,3) in Pb–Pb collisions at  $\sqrt{s_{NN}} = 2.76$  TeV are compared to various AMPT models. Upper panels are the results of SC( $m,n$ ) and the lower panels are the results of NSC( $m,n$ ).

Ref. [79] based on a AMPT model. NSC( $m,n$ ) correlators increase with the larger  $\eta/s$  in hydrodynamic calculations in 0-30% centrality range in the same way as the event plane correlations [80, 81]. In semi-peripheral collisions ( $>40\%$ ), the opposite trend is observed.

We list here important findings from the model comparison:

- (i) All the VISH2+1 model calculations with large  $\eta/s$  regardless of the initial conditions failed to capture the centrality dependence of correlations.
- (ii) Among the VISH2+1 model calculations with small  $\eta/s$  ( $\eta/s = 0.08$ ), the one with the AMPT initial condition describes the data better in general but it cannot describe the data quantitatively for most of the centrality ranges.
- (iii) NSC(3,2) observable is sensitive mainly to the initial conditions, while the other observables are sensitive to both the initial conditions and the temperature dependence of  $\eta/s$ .
- (iv) The correlation strength between  $v_3$  and  $v_2$  and between  $v_4$  and  $v_3$  (NSC(3,2) and NSC(4,3)) is significantly underestimated in hydrodynamic model calculations.
- (v) The sign of NSC(3,2) in 0-10% central collisions was found to be different between the data and hydrodynamic model calculations while the default AMPT model can reproduce the sign.
- (vi) The default AMPT model can describe the normalized symmetric cumulants (NSC( $m,n$ )) quantitatively for most of centralities while the string melting AMPT model fails to describe them.
- (vii) A hierarchy NSC(5,3) > NSC(4,2) > NSC(5,2) holds for centrality ranges  $> 20\%$  within the errors. This hierarchy is well reproduced both by hydrodynamic and AMPT model calculations.

### 6.3 Transverse Momentum Dependence of Correlations between $v_2$ , $v_3$ and $v_4$

It can be seen in Fig. 2 that the  $p_T$  dependence for NSC(3,2) is not clearly seen and it is consistent with no  $p_T$  dependence for the centrality range  $<30\%$  and shows moderate decreasing trend for increasing  $p_T$  for  $>30\%$  centrality range. NSC(4,2) shows a moderate decreasing trend as  $p_T$  or the centrality increase.

In order to see the trend more clearly, we show  $NSC(m,n)$  results as a function of minimum  $p_T$  cut in Fig. 8.

$NSC(3,2)$  and  $NSC(4,2)$  as a function of different minimum  $p_T$  cut are compared to the AMPT simulations in Fig. 8. These observed  $p_T$  dependence for  $NSC(3,2)$  and  $NSC(4,2)$  in mid-central collisions is seen also in AMPT simulations for higher minimum  $p_T$  cuts. The other AMPT configurations except for the default AMPT model give very strong  $p_T$  dependence above 1 GeV/c and cannot describe the magnitude of the data both for  $NSC(3,2)$  and  $NSC(4,2)$  simultaneously. In the case of  $NSC(3,2)$ , the default AMPT model describes the magnitude and  $p_T$  dependence well in all collision centralities except for 40 – 50% where the model underestimates the data and have stronger  $p_T$  dependence than the data. As for  $NSC(4,2)$ , the same model which describes  $NSC(3,2)$  also can reproduce the data well except for 10 – 20% and 40 – 50% centralities where some deviations from the data both for the magnitude and  $p_T$  dependence are observed. When the string melting AMPT model is compared to the same model with the hadronic rescattering off, it is observed that the very strong  $p_T$  dependence as well as the correlation strength gets weaker by the hadronic rescattering. This might imply that the hadronic interaction is the source of this observed  $p_T$  dependence even though the relative contributions from partonic and hadronic stage in the final state particle should be studied further.

The event-by-event EKRT+viscous hydrodynamic calculations are compared to the data in Fig. 8. As it has been discussed,  $NSC(3,2)$  is underestimated by the hydrodynamic calculations. Hence we focus on the  $p_T$  dependence.

This observed moderate  $p_T$  dependence in mid-central collisions both for  $NSC(3,2)$  and  $NSC(4,2)$  might be an indication of possible viscous corrections for the equilibrium distribution at hadronic freeze-out predicted in [37]. The comparisons to hydrodynamic models can further help to understand the viscous correction to the momentum distribution at hadronic freeze-out [30, 36].

## 7 Summary

In this article, we report the centrality dependence of correlation between the higher order harmonics ( $v_3, v_4, v_5$ ) and the lower order harmonics ( $v_2, v_3$ ) as well as the transverse momentum dependence of  $v_3-v_2$  and  $v_4-v_2$  correlations. The results are obtained by the Symmetric 2-harmonic 4-particle Cumulants (SC). It was demonstrated earlier in [38] that this method is insensitive to the non-flow effects and free from symmetry plane correlations. We have found that fluctuations of  $v_3-v_2$  and  $v_4-v_3$  are anti-correlated in all centralities while fluctuations of  $v_4-v_2, v_5-v_2$  and  $v_5-v_3$  are correlated for all centralities. This measurement were compared to various hydrodynamic model calculations with different initial conditions as well as different parameterizations of the temperature dependence of  $\eta/s$ . It is found that the different order harmonic correlations have different sensitivities to the initial conditions and the system properties. Therefore they have discriminating power in separating the effects of  $\eta/s$  from the initial conditions to the final state particle anisotropies. The sign of  $v_3-v_2$  correlation in 0-10% central collisions was found to be different between the data and hydrodynamic model calculations. In the most central collisions the anisotropies originate mainly from fluctuations, where the initial ellipsoidal geometry which is dominating in mid-central collisions plays little role. This observation might help to understand the details of the fluctuations in initial conditions. The comparisons to VISH2+1 calculation show that all the models with large  $\eta/s$  regardless of the initial conditions failed to capture the centrality dependence of higher order correlations, more clearly than lower order harmonic correlations. Based on the tested model parameters, the  $\eta/s$  should be small and AMPT initial condition is favored by the data. A quite clear separation of the correlation strength between different initial conditions is observed for these higher order harmonic correlations compared to the lower order harmonic correlations. The default configuration of AMPT model describes well the normalized symmetric cumulants ( $NSC(m,n)$ ) for most of centralities and for most combinations of harmonics which were considered. Together with the measurements of individual

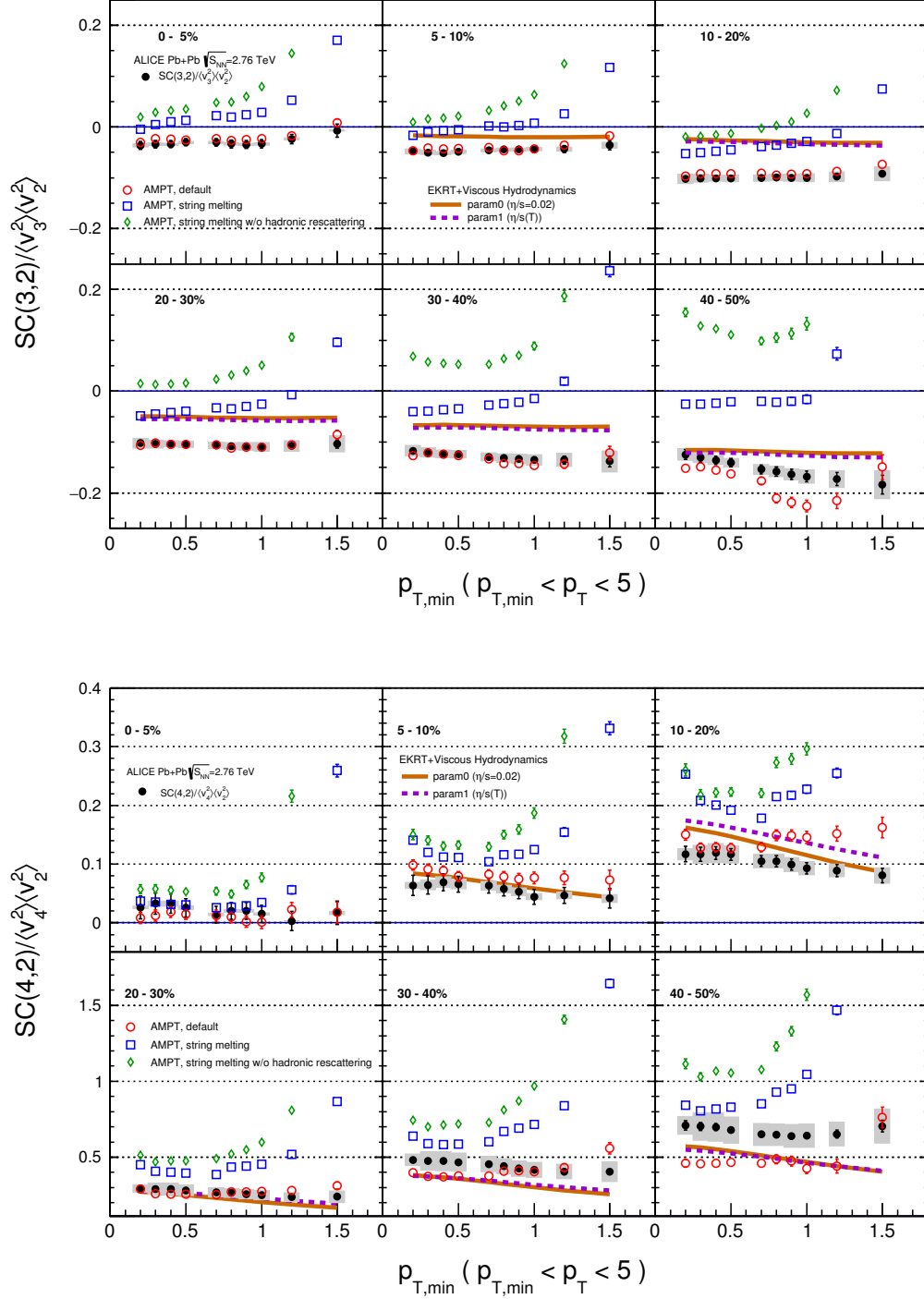


**Fig. 8:** NSC(3,2) (Top) and NSC(4,2) (Bottom) as a function of minimum  $p_T$  cuts in Pb-Pb collisions at  $\sqrt{s_{NN}} = 2.76$  TeV are compared to various AMPT models and event-by-event EKRT+viscous hydrodynamic calculations [30].

harmonics these results provide further constraints on the system properties and help discriminating between theoretical models. Finally, we have found that  $v_3$  and  $v_2$ ,  $v_4$  and  $v_2$  correlations have moderate  $p_T$  dependence in mid-central collisions. This might be an indication of possible viscous corrections for the equilibrium distribution at hadronic freeze-out. The results presented in this article can be used to further optimize model parameters and put better constraints on the initial conditions and the transport properties of nuclear matter in ultra-relativistic heavy-ion collisions.

## Acknowledgements

## References

- [1] **STAR** Collaboration, K. H. Ackermann *et al.*, “Elliptic flow in Au + Au collisions at  $(S(NN))^{1/2} = 130$  GeV,” *Phys. Rev. Lett.* **86** (2001) 402–407, arXiv:nuc1-ex/0009011 [nuc1-ex].
- [2] **ALICE** Collaboration, K. Aamodt *et al.*, “Elliptic flow of charged particles in Pb-Pb collisions at 2.76 TeV,” *Phys. Rev. Lett.* **105** (2010) 252302, arXiv:1011.3914 [nuc1-ex].
- [3] **ALICE** Collaboration, J. Adam *et al.*, “Anisotropic flow of charged particles in Pb-Pb collisions at  $\sqrt{s_{NN}} = 5.02$  TeV,” *Phys. Rev. Lett.* **116** no. 13, (2016) 132302, arXiv:1602.01119 [nuc1-ex].
- [4] P. Romatschke and U. Romatschke, “Viscosity Information from Relativistic Nuclear Collisions: How Perfect is the Fluid Observed at RHIC?,” *Phys. Rev. Lett.* **99** (2007) 172301, arXiv:0706.1522 [nuc1-th].
- [5] C. Shen, U. Heinz, P. Huovinen, and H. Song, “Radial and elliptic flow in Pb+Pb collisions at the Large Hadron Collider from viscous hydrodynamic,” *Phys. Rev.* **C84** (2011) 044903, arXiv:1105.3226 [nuc1-th].
- [6] B. Schenke, S. Jeon, and C. Gale, “Elliptic and triangular flows in 3 + 1D viscous hydrodynamics with fluctuating initial conditions,” *J. Phys.* **G38** (2011) 124169.
- [7] P. Bozek and I. Wyskiel-Piekarska, “Particle spectra in Pb-Pb collisions at  $\sqrt{s_{NN}} = 2.76$  TeV,” *Phys. Rev.* **C85** (2012) 064915, arXiv:1203.6513 [nuc1-th].
- [8] “Event-by-event anisotropic flow in heavy-ion collisions from combined Yang-Mills and viscous fluid dynamics,” *Phys. Rev. Lett.* **110** no. 1, (2013) 012302, arXiv:1209.6330 [nuc1-th].
- [9] T. Hirano, P. Huovinen, and Y. Nara, “Elliptic flow in Pb+Pb collisions at  $\sqrt{s_{NN}} = 2.76$  TeV: hybrid model assessment of the first data,” *Phys. Rev.* **C84** (2011) 011901, arXiv:1012.3955 [nuc1-th].
- [10] P. Kovtun, D. T. Son, and A. O. Starinets, “Viscosity in strongly interacting quantum field theories from black hole physics,” *Phys. Rev. Lett.* **94** (2005) 111601, arXiv:hep-th/0405231 [hep-th].
- [11] R. A. Lacey, N. N. Ajitanand, J. M. Alexander, P. Chung, W. G. Holzmann, M. Issah, A. Taranenko, P. Danielewicz, and H. Stoecker, “Has the QCD Critical Point been Signaled by Observations at RHIC?,” *Phys. Rev. Lett.* **98** (2007) 092301, arXiv:nuc1-ex/0609025 [nuc1-ex].
- [12] P. Danielewicz and M. Gyulassy, “Dissipative phenomena in quark-gluon plasmas,” *Phys. Rev. D* **31** (Jan, 1985) 53–62. <http://link.aps.org/doi/10.1103/PhysRevD.31.53>.



- [13] L. P. Csernai, J. Kapusta, and L. D. McLerran, “On the Strongly-Interacting Low-Viscosity Matter Created in Relativistic Nuclear Collisions,” *Phys. Rev. Lett.* **97** (2006) 152303, arXiv:nucl-th/0604032 [nucl-th].
- [14] J.-Y. Ollitrault, “Anisotropy as a signature of transverse collective flow,” *Phys. Rev.* **D46** (1992) 229–245.
- [15] S. Voloshin and Y. Zhang, “Flow study in relativistic nuclear collisions by Fourier expansion of Azimuthal particle distributions,” *Z. Phys.* **C70** (1996) 665–672, arXiv:hep-ph/9407282 [hep-ph].
- [16] S. Floerchinger, U. A. Wiedemann, A. Beraudo, L. Del Zanna, G. Inghirami, and V. Rolando, “How (non-)linear is the hydrodynamics of heavy ion collisions?,” *Phys. Lett.* **B735** (2014) 305–310, arXiv:1312.5482 [hep-ph].
- [17] M. Miller and R. Snellings, “Eccentricity fluctuations and its possible effect on elliptic flow measurements,” arXiv:nucl-ex/0312008 [nucl-ex].
- [18] **PHOBOS** Collaboration, B. Alver *et al.*, “System size, energy, pseudorapidity, and centrality dependence of elliptic flow,” *Phys. Rev. Lett.* **98** (2007) 242302, arXiv:nucl-ex/0610037 [nucl-ex].
- [19] B. Alver and G. Roland, “Collision geometry fluctuations and triangular flow in heavy-ion collisions,” *Phys. Rev.* **C81** (2010) 054905, arXiv:1003.0194 [nucl-th]. [Erratum: *Phys. Rev.* **C82**, 039903(2010)].
- [20] **ALICE** Collaboration, K. Aamodt *et al.*, “Higher harmonic anisotropic flow measurements of charged particles in Pb-Pb collisions at  $\sqrt{s_{NN}}=2.76$  TeV,” *Phys. Rev. Lett.* **107** (2011) 032301, arXiv:1105.3865 [nucl-ex].
- [21] H. Niemi, G. S. Denicol, H. Holopainen, and P. Huovinen, “Event-by-event distributions of azimuthal asymmetries in ultrarelativistic heavy-ion collisions,” *Phys. Rev.* **C87** no. 5, (2013) 054901, arXiv:1212.1008 [nucl-th].
- [22] **ATLAS** Collaboration, G. Aad *et al.*, “Measurement of event-plane correlations in  $\sqrt{s_{NN}} = 2.76$  TeV lead-lead collisions with the ATLAS detector,” *Phys. Rev.* **C90** no. 2, (2014) 024905, arXiv:1403.0489 [hep-ex].
- [23] B. H. Alver, C. Gombeaud, M. Luzum, and J.-Y. Ollitrault, “Triangular flow in hydrodynamics and transport theory,” *Phys. Rev.* **C82** (2010) 034913, arXiv:1007.5469 [nucl-th].
- [24] M. Luzum and J.-Y. Ollitrault, “Extracting the shear viscosity of the quark-gluon plasma from flow in ultra-central heavy-ion collisions,” *Nucl. Phys.* **A904-905** (2013) 377c–380c, arXiv:1210.6010 [nucl-th].
- [25] C. Shen, S. A. Bass, T. Hirano, P. Huovinen, Z. Qiu, H. Song, and U. Heinz, “The QGP shear viscosity: Elusive goal or just around the corner?,” *J. Phys.* **G38** (2011) 124045, arXiv:1106.6350 [nucl-th].
- [26] P. Bozek, “Flow and interferometry in 3+1 dimensional viscous hydrodynamics,” *Phys. Rev.* **C85** (2012) 034901, arXiv:1110.6742 [nucl-th].
- [27] J.-B. Rose, J.-F. Paquet, G. S. Denicol, M. Luzum, B. Schenke, S. Jeon, and C. Gale, “Extracting the bulk viscosity of the quark-gluon plasma,” *Nucl. Phys.* **A931** (2014) 926–930, arXiv:1408.0024 [nucl-th].

- [28] S. Ryu, J. F. Paquet, C. Shen, G. S. Denicol, B. Schenke, S. Jeon, and C. Gale, “Importance of the Bulk Viscosity of QCD in Ultrarelativistic Heavy-Ion Collisions,” *Phys. Rev. Lett.* **115** no. 13, (2015) 132301, arXiv:1502.01675 [nucl-th].
- [29] D. Teaney and L. Yan, “Triangularity and Dipole Asymmetry in Heavy Ion Collisions,” *Phys. Rev.* **C83** (2011) 064904, arXiv:1010.1876 [nucl-th].
- [30] H. Niemi, K. J. Eskola, and R. Paatelainen, “Event-by-event fluctuations in a perturbative QCD + saturation + hydrodynamics model: Determining QCD matter shear viscosity in ultrarelativistic heavy-ion collisions,” *Phys. Rev.* **C93** no. 2, (2016) 024907, arXiv:1505.02677 [hep-ph].
- [31] Z. Qiu and U. W. Heinz, “Event-by-event shape and flow fluctuations of relativistic heavy-ion collision fireballs,” *Phys. Rev.* **C84** (2011) 024911, arXiv:1104.0650 [nucl-th].
- [32] S. S. Gubser and A. Yarom, “Conformal hydrodynamics in Minkowski and de Sitter spacetimes,” *Nucl. Phys.* **B846** (2011) 469–511, arXiv:1012.1314 [hep-th].
- [33] Y. Hatta, J. Noronha, G. Torrieri, and B.-W. Xiao, “Flow harmonics within an analytically solvable viscous hydrodynamic model,” *Phys. Rev.* **D90** no. 7, (2014) 074026, arXiv:1407.5952 [hep-ph].
- [34] L. V. Bravina, B. H. Bruchheim Johansson, G. K. Eyyubova, V. L. Korotkikh, I. P. Lokhtin, L. V. Malinina, S. V. Petrushanko, A. M. Snigirev, and E. E. Zabrodin, “Higher harmonics of azimuthal anisotropy in relativistic heavy ion collisions in HYDJET++ model,” *Eur. Phys. J.* **C74** no. 3, (2014) 2807, arXiv:1311.7054 [nucl-th].
- [35] L. V. Bravina, B. H. Bruchheim Johansson, G. K. Eyyubova, V. L. Korotkikh, I. P. Lokhtin, L. V. Malinina, S. V. Petrushanko, A. M. Snigirev, and E. E. Zabrodin, “Hexagonal flow  $v_6$  as a superposition of elliptic  $v_2$  and triangular  $v_3$  flows,” *Phys. Rev.* **C89** no. 2, (2014) 024909, arXiv:1311.0747 [hep-ph].
- [36] D. Teaney and L. Yan, “Non linearities in the harmonic spectrum of heavy ion collisions with ideal and viscous hydrodynamics,” *Phys. Rev.* **C86** (2012) 044908, arXiv:1206.1905 [nucl-th].
- [37] M. Luzum and J.-Y. Ollitrault, “Constraining the viscous freeze-out distribution function with data obtained at the BNL Relativistic Heavy Ion Collider (RHIC),” *Phys. Rev.* **C82** (2010) 014906, arXiv:1004.2023 [nucl-th].
- [38] ALICE Collaboration, J. Adam *et al.*, “Correlated event-by-event fluctuations of flow harmonics in Pb-Pb collisions at  $\sqrt{s_{NN}} = 2.76$  TeV,” *Phys. Rev. Lett.* **117** (2016) 182301, arXiv:1604.07663 [nucl-ex].
- [39] X. Zhu, Y. Zhou, H. Xu, and H. Song, “Correlations of flow harmonics in 2.76A TeV Pb–Pb collisions,” arXiv:1608.05305 [nucl-th].
- [40] H. Niemi, G. S. Denicol, P. Huovinen, E. Molnar, and D. H. Rischke, “Influence of the shear viscosity of the quark-gluon plasma on elliptic flow in ultrarelativistic heavy-ion collisions,” *Phys. Rev. Lett.* **106** (2011) 212302, arXiv:1101.2442 [nucl-th].
- [41] A. Bilandzic, C. H. Christensen, K. Gulbrandsen, A. Hansen, and Y. Zhou, “Generic framework for anisotropic flow analyses with multiparticle azimuthal correlations,” *Phys. Rev.* **C89** no. 6, (2014) 064904, arXiv:1312.3572 [nucl-ex].
- [42] G. Giacalone, L. Yan, J. Noronha-Hostler, and J.-Y. Ollitrault, “Symmetric cumulants and event-plane correlations in Pb + Pb collisions,” *Phys. Rev.* **C94** no. 1, (2016) 014906, arXiv:1605.08303 [nucl-th].

- [43] **ALICE** Collaboration, K. Aamodt *et al.*, “The ALICE experiment at the CERN LHC,” *JINST* **3** (2008) S08002.
- [44] **ALICE** Collaboration, P. Cortese *et al.*, “ALICE: Physics performance report, volume I,” *J. Phys.* **G30** (2004) 1517–1763.
- [45] **ALICE** Collaboration, P. Cortese *et al.*, “ALICE: Physics performance report, volume II,” *J. Phys.* **G32** (2006) 1295–2040.
- [46] **ALICE** Collaboration, K. Aamodt *et al.*, “Centrality dependence of the charged-particle multiplicity density at mid-rapidity in Pb-Pb collisions at  $\sqrt{s_{NN}} = 2.76$  TeV,” *Phys. Rev. Lett.* **106** (2011) 032301, arXiv:1012.1657 [nucl-ex].
- [47] X.-N. Wang and M. Gyulassy, “HIJING: A Monte Carlo model for multiple jet production in p p, p A and A A collisions,” *Phys. Rev.* **D44** (1991) 3501–3516.
- [48] “GEANT Detector Description and Simulation Tool,”.
- [49] **ALICE** Collaboration, E. Abbas *et al.*, “Performance of the ALICE VZERO system,” *JINST* **8** (2013) P10016, arXiv:1306.3130 [nucl-ex].
- [50] **ALICE** Collaboration, G. Dellacasa *et al.*, “ALICE technical design report of the inner tracking system (ITS),”.
- [51] S. A. Voloshin, A. M. Poskanzer, and R. Snellings, “Collective phenomena in non-central nuclear collisions,” arXiv:0809.2949 [nucl-ex].
- [52] **ALICE** Collaboration, B. Abelev *et al.*, “Anisotropic flow of charged hadrons, pions and (anti-)protons measured at high transverse momentum in Pb-Pb collisions at  $\sqrt{s_{NN}}=2.76$  TeV,” *Phys. Lett.* **B719** (2013) 18–28, arXiv:1205.5761 [nucl-ex].
- [53] R. Paatelainen, K. J. Eskola, H. Holopainen, and K. Tuominen, “Multiplicities and  $p_T$  spectra in ultrarelativistic heavy ion collisions from a next-to-leading order improved perturbative QCD + saturation + hydrodynamics model,” *Phys. Rev.* **C87** no. 4, (2013) 044904, arXiv:1211.0461 [hep-ph].
- [54] R. Paatelainen, K. J. Eskola, H. Niemi, and K. Tuominen, “Fluid dynamics with saturated minijet initial conditions in ultrarelativistic heavy-ion collisions,” *Phys. Lett.* **B731** (2014) 126–130, arXiv:1310.3105 [hep-ph].
- [55] C. Shen, U. Heinz, P. Huovinen, and H. Song, “Systematic parameter study of hadron spectra and elliptic flow from viscous hydrodynamic simulations of Au+Au collisions at  $\sqrt{s_{NN}} = 200$  GeV,” *Phys. Rev.* **C82** (2010) 054904, arXiv:1010.1856 [nucl-th].
- [56] C. Shen, Z. Qiu, H. Song, J. Bernhard, S. Bass, and U. Heinz, “The iEBE-VISHNU code package for relativistic heavy-ion collisions,” *Comput. Phys. Commun.* **199** (2016) 61–85, arXiv:1409.8164 [nucl-th].
- [57] Z. Qiu, C. Shen, and U. Heinz, “Hydrodynamic elliptic and triangular flow in Pb-Pb collisions at  $\sqrt{s} = 2.76$  ATeV,” *Phys. Lett.* **B707** (2012) 151–155, arXiv:1110.3033 [nucl-th].
- [58] R. S. Bhalerao, A. Jaiswal, and S. Pal, “Collective flow in event-by-event partonic transport plus hydrodynamics hybrid approach,” *Phys. Rev.* **C92** no. 1, (2015) 014903, arXiv:1503.03862 [nucl-th].

- [59] P. F. Kolb, J. Sollfrank, and U. W. Heinz, “Anisotropic transverse flow and the quark hadron phase transition,” *Phys. Rev.* **C62** (2000) 054909, arXiv:hep-ph/0006129 [hep-ph].
- [60] D. Kharzeev and M. Nardi, “Hadron production in nuclear collisions at RHIC and high density QCD,” *Phys. Lett.* **B507** (2001) 121–128, arXiv:nucl-th/0012025 [nucl-th].
- [61] M. L. Miller, K. Reygers, S. J. Sanders, and P. Steinberg, “Glauber modeling in high energy nuclear collisions,” *Ann. Rev. Nucl. Part. Sci.* **57** (2007) 205–243, arXiv:nucl-ex/0701025 [nucl-ex].
- [62] H. J. Drescher and Y. Nara, “Effects of fluctuations on the initial eccentricity from the Color Glass Condensate in heavy ion collisions,” *Phys. Rev.* **C75** (2007) 034905, arXiv:nucl-th/0611017 [nucl-th].
- [63] T. Hirano and Y. Nara, “Eccentricity fluctuation effects on elliptic flow in relativistic heavy ion collisions,” *Phys. Rev.* **C79** (2009) 064904, arXiv:0904.4080 [nucl-th].
- [64] L. Pang, Q. Wang, and X.-N. Wang, “Effects of initial flow velocity fluctuation in event-by-event (3+1)D hydrodynamics,” *Phys. Rev.* **C86** (2012) 024911, arXiv:1205.5019 [nucl-th].
- [65] H.-j. Xu, Z. Li, and H. Song, “High-order flow harmonics of identified hadrons in 2.76A TeV Pb + Pb collisions,” *Phys. Rev.* **C93** no. 6, (2016) 064905, arXiv:1602.02029 [nucl-th].
- [66] B. Zhang, C. M. Ko, B.-A. Li, and Z.-w. Lin, “A multiphase transport model for nuclear collisions at RHIC,” *Phys. Rev.* **C61** (2000) 067901, arXiv:nucl-th/9907017 [nucl-th].
- [67] Z.-w. Lin, S. Pal, C. M. Ko, B.-A. Li, and B. Zhang, “Charged particle rapidity distributions at relativistic energies,” *Phys. Rev.* **C64** (2001) 011902, arXiv:nucl-th/0011059 [nucl-th].
- [68] Z.-W. Lin, C. M. Ko, B.-A. Li, B. Zhang, and S. Pal, “A Multi-phase transport model for relativistic heavy ion collisions,” *Phys. Rev.* **C72** (2005) 064901, arXiv:nucl-th/0411110 [nucl-th].
- [69] A. Kurkela and Y. Zhu, “Isotropization and hydrodynamization in weakly coupled heavy-ion collisions,” *Phys. Rev. Lett.* **115** no. 18, (2015) 182301, arXiv:1506.06647 [hep-ph].
- [70] M. Gyulassy and X.-N. Wang, “HIJING 1.0: A Monte Carlo program for parton and particle production in high-energy hadronic and nuclear collisions,” *Comput. Phys. Commun.* **83** (1994) 307, arXiv:nucl-th/9502021 [nucl-th].
- [71] B. Andersson, G. Gustafson, and B. Nilsson-Almqvist, “A Model for Low p(t) Hadronic Reactions, with Generalizations to Hadron - Nucleus and Nucleus-Nucleus Collisions,” *Nucl. Phys.* **B281** (1987) 289–309.
- [72] B. Nilsson-Almqvist and E. Stenlund, “Interactions Between Hadrons and Nuclei: The Lund Monte Carlo, Fritiof Version 1.6,” *Comput. Phys. Commun.* **43** (1987) 387.
- [73] B. Zhang, “ZPC 1.0.1: A Parton cascade for ultrarelativistic heavy ion collisions,” *Comput. Phys. Commun.* **109** (1998) 193–206, arXiv:nucl-th/9709009 [nucl-th].
- [74] B. Li, A. T. Sustich, B. Zhang, and C. M. Ko, “Studies of superdense hadronic matter in a relativistic transport model,” *Int. J. Mod. Phys.* **E10** (2001) 267–352.
- [75] Z.-w. Lin and C. M. Ko, “Partonic effects on the elliptic flow at RHIC,” *Phys. Rev.* **C65** (2002) 034904, arXiv:nucl-th/0108039 [nucl-th].

- [76] Z.-W. Lin, “Evolution of transverse flow and effective temperatures in the parton phase from a multi-phase transport model,” *Phys. Rev.* **C90** no. 1, (2014) 014904, arXiv:1403.6321 [nucl-th].
- [77] **ALICE** Collaboration, J. Adam *et al.*, “Higher harmonic flow coefficients of identified hadrons in Pb-Pb collisions at  $\sqrt{s_{NN}} = 2.76$  TeV,” *JHEP* **09** (2016) 164, arXiv:1606.06057 [nucl-ex].
- [78] **ATLAS** Collaboration, G. Aad *et al.*, “Measurement of the distributions of event-by-event flow harmonics in lead-lead collisions at  $\sqrt{s_{NN}} = 2.76$  TeV with the ATLAS detector at the LHC,” *JHEP* **11** (2013) 183, arXiv:1305.2942 [hep-ex].
- [79] R. S. Bhalerao, J.-Y. Ollitrault, and S. Pal, “Characterizing flow fluctuations with moments,” *Phys. Lett.* **B742** (2015) 94–98, arXiv:1411.5160 [nucl-th].
- [80] R. S. Bhalerao, J.-Y. Ollitrault, and S. Pal, “Event-plane correlators,” *Phys. Rev.* **C88** (2013) 024909, arXiv:1307.0980 [nucl-th].
- [81] D. Teaney and L. Yan, “Event-plane correlations and hydrodynamic simulations of heavy ion collisions,” *Phys. Rev.* **C90** no. 2, (2014) 024902, arXiv:1312.3689 [nucl-th].
- [82] **ATLAS** Collaboration, G. Aad *et al.*, “Measurement with the ATLAS detector of multi-particle azimuthal correlations in p+Pb collisions at  $\sqrt{s_{NN}} = 5.02$  TeV,” *Phys. Lett.* **B725** (2013) 60–78, arXiv:1303.2084 [hep-ex].
- [83] **ALICE** Collaboration, B. B. Abelev *et al.*, “Multiparticle azimuthal correlations in p-Pb and Pb-Pb collisions at the CERN Large Hadron Collider,” *Phys. Rev.* **C90** no. 5, (2014) 054901, arXiv:1406.2474 [nucl-ex].
- [84] **CMS** Collaboration, V. Khachatryan *et al.*, “Evidence for Collective Multiparticle Correlations in p-Pb Collisions,” *Phys. Rev. Lett.* **115** no. 1, (2015) 012301, arXiv:1502.05382 [nucl-ex].
- [85] **STAR** Collaboration, L. Adamczyk *et al.*, “Long-range pseudorapidity dihadron correlations in d+Au collisions at  $\sqrt{s_{NN}} = 200$  GeV,” *Phys. Lett.* **B747** (2015) 265–271, arXiv:1502.07652 [nucl-ex].
- [86] **PHENIX** Collaboration, A. Adare *et al.*, “Measurements of elliptic and triangular flow in high-multiplicity  $^3\text{He}+\text{Au}$  collisions at  $\sqrt{s_{NN}} = 200$  GeV,” *Phys. Rev. Lett.* **115** no. 14, (2015) 142301, arXiv:1507.06273 [nucl-ex].
- [87] C. Loizides, “Experimental overview on small collision systems at the LHC,” in *Proceedings, 25th International Conference on Ultra-Relativistic Nucleus-Nucleus Collisions (Quark Matter 2015): Kobe, Japan, September 27-October 3, 2015*. 2016. arXiv:1602.09138 [nucl-ex].  
<https://inspirehep.net/record/1424892/files/arXiv:1602.09138.pdf>.

**693 A The ALICE Collaboration**